ARTICLE IN PRESS

Computers and Mathematics with Applications ▮ (▮▮▮▮) ▮▮▮–▮▮▮

Contents lists available at ScienceDirect

Computers and Mathematics with Applications

journal homepage: www.elsevier.com/locate/camwa

On the virtual element method for topology optimization on polygonal meshes: A numerical study☆

P.F. Antonietti [a], M. Bruggi [b], S. Scacchi [c,*], M. Verani [a]

[a] MOX, Dipartimento di Matematica, Politecnico di Milano, Italy
[b] Dipartimento di Ingegneria Civile e Ambientale, Politecnico di Milano, Italy
[c] Dipartimento di Matematica, Università degli Studi di Milano, Italy

ARTICLE INFO

Article history:
Available online xxxx

Keywords:
Virtual element method
Topology optimization
Linear elasticity
Stokes equations

ABSTRACT

It is well known that the solution of topology optimization problems may be affected both by the geometric properties of the computational mesh, which can steer the minimization process towards local (and non-physical) minima, and by the accuracy of the method employed to discretize the underlying differential problem, which may not be able to correctly capture the physics of the problem. In light of the above remarks, in this paper we consider polygonal meshes and employ the virtual element method (VEM) to solve two classes of paradigmatic topology optimization problems, one governed by nearly-incompressible and compressible linear elasticity and the other by Stokes equations. Several numerical results show the virtues of our polygonal VEM based approach with respect to more standard methods.

1. Introduction

The study of numerical methods for the approximation of partial differential equations on polygonal and polyhedral meshes is drawing the attention of an increasing number of researchers (see, e.g., the special issues [1,2] for a recent overview of the different methodologies). Among the different proposed methodologies, here we focus on the Virtual Element Method (VEM) which has been introduced in the pioneering paper [3] and can be seen as an evolution of the Mimetic Finite Difference method, see, e.g., [4,5] for a detailed description. Recently, VEM has been analyzed for general elliptic problems [6,7], linear and nonlinear elasticity [8–10], plate bending [11,12], Cahn–Hilliard [13], Stokes [14,15], Helmholtz [16], parabolic [17], Steklov eigenvalue [18], elliptic eigenvalue [19] and discrete fracture networks [20]. In parallel, several different variants of the VEM have been proposed and analyzed: mixed [21,22], discontinuous [23], $H(\mathrm{div})$ and $H(\mathbf{curl})$-conforming [24], hp [25], serendipity [26] and nonconforming [27–31] VEM.

Such a flourishing research activity founds an important motivation in the great flexibility that the use of polytopal meshes can ensure in dealing with problems posed on very complicated and possibly deformable geometries. In this respect, as first recognized by G.H. Paulino and his collaborators in a series of ground breaking papers [32–36], topology optimization represents an intriguing challenge for the use of polyhedral meshes. Topology optimization is a fertile area of research

☆ Paola F. Antonietti has been partially supported by the SIR Starting Grant no. RBSI14VT0S "PolyPDEs: Non-conforming polyhedral finite element methods for the approximation of partial differential equations" funded by MIUR - Italian Ministry of Education, Universities and Research. M. Verani has been partially supported by the Italian research grant Prin 2012 2012HBLYE4 "Metodologie innovative nella modellistica differenziale numerica" and by INdAM-GNCS.

* Corresponding author.
E-mail addresses: paola.antonietti@polimi.it (P.F. Antonietti), matteo.bruggi@polimi.it (M. Bruggi), simone.scacchi@unimi.it (S. Scacchi), marco.verani@polimi.it (M. Verani).

http://dx.doi.org/10.1016/j.camwa.2017.05.025
0898-1221/

that is mainly concerned with the automatic generation of optimal layouts to solve design problems in Engineering. The classical formulation addresses the problem of finding the best distribution of an isotropic material that minimizes the work of the external loads at equilibrium, while respecting a constraint on the assigned amount of volume. This is the so-called minimum compliance formulation that can be conveniently employed to achieve stiff truss-like layout within a two-dimensional domain. A classical implementation resorts to the adoption of four node (displacement-based) finite elements that are coupled with an elementwise discretization of the (unknown) density field. When regular meshes made of square elements are used, well-known numerical instabilities arise, see in particular the so-called checkerboard patterns. On the other hand, when unstructured meshes are needed to cope with complex geometries, additional instabilities can steer the optimizer towards local minima instead of the expected global one. Unstructured meshes approximate the strain energy of truss-like members with an accuracy that is strictly related to the geometrical features of the discretization, thus remarkably affecting the achieved layouts. On this latter issue, as pointed out also in [32], the use of polyhedral meshes provides flexibility in the difficult computational task of meshing complex geometries, while, in parallel, it can contribute to avoid that the geometry of the mesh dictates the possible layout of material and the orientation of members, thus excluding physical optimal configurations from the final design obtained by the numerical procedure.

The aim of this paper is to push forward the study of [32,35,36]. In [32] the authors analyze the possibility of avoiding sub-optimal (non-physical) layout in topology optimization for structural applications when *polygonal finite elements* and polytopal meshes are employed, whereas in [36] the virtual element method is employed for solving compliance minimization and compliant mechanism problems in three dimensions. In [35] *polygonal finite elements* are employed to solve topology optimization problems governed by Stokes equations on polygonal meshes. In view of the above contributions, and with the goal of deepening the comprehension of the role of VEM and polygonal meshes in topology optimization, we focus on the use of this latter method for solving topology optimization governed by linear elasticity (compressible and nearly-incompressible) and Stokes flow. For each of the above examples, we systematically consider the impact that the combined approach VEM and polygonal meshes has on the quality of the obtained layout and compare them with the ones provided by standard approaches.

The outline of the paper is the following. In Section 2 we present the continuous formulation of the topology optimization problems that we will consider throughout the paper, while in Section 3 we introduce the corresponding virtual element discretizations. In Section 4 we present and extensively discuss several numerical experiments assessing the virtues of the combined use of VEM and polygonal meshes in solving each of the previously introduced topology optimization problems. Finally, in Section 5 we draw some conclusion.

2. Topology optimization problems: continuous formulation

We briefly recall the continuous formulations of the topology optimization problems we are interested in, namely the minimum compliance problem governed by the linear elasticity equation (Section 2.1) and the optimal flow problem governed by the Stokes equation (Section 2.2). We first recall some notation that will be useful in the following. Let Ω be a two-dimensional bounded, polygonal domain with boundary $\Gamma = \partial\Omega$ and let $\Gamma_d \subset \Gamma$ be a subset of the boundary of the domain. We introduce the following spaces

$$\mathcal{V}_0 = \{\mathbf{u} \in (H^1(\Omega))^2 : \mathbf{u} = \mathbf{0} \text{ on } \Gamma_d\}$$
$$\mathcal{V}_d = \{\mathbf{u} \in (H^1(\Omega))^2 : \mathbf{u} = \mathbf{u_d} \text{ on } \Gamma_d\}$$

where $\mathbf{u_d}$ is a possibly null given function. Moreover, let us introduce the control space

$$\mathcal{Q}_{\text{ad}} = \{\rho \in L^\infty(\Omega) : 0 < \rho_{\min} \leq \rho \leq 1 \text{ a.e. in } \Omega\}$$

of bounded functions representing the material density in Ω, where $\rho_{\min}$ is some positive lower bound.

2.1. Minimum compliance

In this section we shortly describe the topology optimization problem for minimum compliance. This corresponds to find the optimal distribution of a given amount of linear elastic isotropic material (described by an element of $\mathcal{Q}_{\text{ad}}$) such that the work of the external load against the corresponding displacement at equilibrium is minimized.

More precisely, let λ_0 and μ_0 be the Lamé coefficients of the given material and introduce the bilinear form $a(\cdot,\cdot) : (H^1(\Omega))^2 \times (H^1(\Omega))^2 \to \mathbb{R}$ defined as follows

$$a(\mathbf{u},\mathbf{v}) = 2\mu_0 \int_\Omega \epsilon(\mathbf{u}) : \epsilon(\mathbf{v})\, d\mathbf{x} + \lambda_0 \int_\Omega \operatorname{div}\mathbf{u} \operatorname{div}\mathbf{v}\, d\mathbf{x}, \tag{1}$$

where $\epsilon(\mathbf{u}) = \frac{1}{2}\left(\nabla\mathbf{u} + \nabla^T\mathbf{u}\right)$ is the symmetric gradient. Moreover, let us introduce the semi-linear form $a(\rho;\cdot,\cdot) : \mathcal{Q}_{\text{ad}} \times (H^1(\Omega))^2 \times (H^1(\Omega))^2 \to \mathbb{R}$

$$a(\rho;\mathbf{u},\mathbf{v}) = 2\int_\Omega \mu(\rho)\epsilon(\mathbf{u}) : \epsilon(\mathbf{v})\, d\mathbf{x} + \int_\Omega \lambda(\rho)\operatorname{div}\mathbf{u} \operatorname{div}\mathbf{v}\, d\mathbf{x} \tag{2}$$

Please cite this article in press as: P.F. Antonietti, et al., On the virtual element method for topology optimization on polygonal meshes: A numerical study, Computers and Mathematics with Applications (2017), http://dx.doi.org/10.1016/j.camwa.2017.05.025.

where, according to the classical SIMP approach, we set $\lambda(\rho) = \lambda_0\rho(x)^{p_\lambda}$ and $\mu(\rho) = \mu_0\rho(x)^{p_\mu}$, being p_λ and p_μ positive parameters (typically equal to 3). Clearly, when $\rho = 1$ in Ω we have $a(\rho; \mathbf{u}, \mathbf{v}) = a(\mathbf{u}, \mathbf{v})$. Finally, let the linear functional $\mathcal{F}(\cdot) : (H^1(\Omega))^2 \to \mathbb{R}$ be defined as

$$\mathcal{F}(\mathbf{v}) = \int_{\Gamma_t} \mathbf{f}_t \cdot \mathbf{v}\, d\mathbf{x}$$

where $\Gamma_t = \Gamma \setminus \Gamma_d$ and the given function $\mathbf{f}_t \in (L^2(\Gamma_t))^2$ represents the external load. In view of the above definitions, given a material distribution described by the function ρ, the elasticity problem (or direct problem) reads as follows: find $\mathbf{u} \in \boldsymbol{\mathcal{V}}_d$ such that

$$a(\rho; \mathbf{u}, \mathbf{v}) = \mathcal{F}(\mathbf{v}) \tag{3}$$

for any $\mathbf{v} \in \boldsymbol{\mathcal{V}}_0$. According to the Clapeyron theorem, the continuous formulation of the topology optimization problem for minimum compliance governed by the elasticity equation can be therefore written as:

$$\begin{cases} \min\limits_{\rho\in\mathcal{Q}_{\text{ad}}} & \mathcal{C}(\rho, \mathbf{u}) = \displaystyle\int_{\Gamma_t} \mathbf{f}_t \cdot \mathbf{u}\, dx \\ \text{s.t.} & a(\rho; \mathbf{u}, \mathbf{v}) = \mathcal{F}(\mathbf{v}) \quad \forall \mathbf{v} \in \boldsymbol{\mathcal{V}}_0 \\ & \dfrac{1}{V}\displaystyle\int_\Omega \rho dx \ \le V_f, \end{cases} \tag{4}$$

being V_f the available amount of material as a fraction of the whole domain $V = \int_\Omega 1 dx$. Minimizing the compliance $\mathcal{C}$ of a structure acted upon by a prescribed set of assigned forces means minimizing the work of external loads, i.e. looking for a stiff structure. When $\lambda_0 \to +\infty$ we refer to (4) as the minimum compliance problem in the case of nearly-incompressible elasticity, otherwise for moderate values of λ_0 we refer to it as the minimum compliance problem in the case of compressible elasticity.

2.2. Optimal Stokes flow

In this section we recall the classical topology optimization problem for optimal Stokes flows [37]: given a design domain Ω with certain boundary conditions, we are interested in determining at what places of Ω there should be fluid or solid in order to minimize a certain energy functional $\mathcal{E}$ (subject to the constraint of the availability of a given amount of fluid). More precisely, let us introduce the bilinear form

$$a(\rho; \mathbf{u}, \mathbf{v}) = 2\mu_0 \int_\Omega \epsilon(\mathbf{u}) : \epsilon(\mathbf{v})\, dx + \lambda_0 \int_\Omega \text{div}\mathbf{u}\, \text{div}\mathbf{v}\, dx + \int_\Omega \alpha(\rho)\mathbf{u}\mathbf{v} \tag{5}$$

where μ_0 is the viscosity of the fluid, λ_0 is a penalty parameter employed to enforce the incompressibility condition and $\alpha(\rho) = \frac{5\mu_0}{\rho^2}$. Given a material distribution described by the function $\rho \in \mathcal{Q}_{\text{ad}}$, the Stokes problem (or direct problem) reads as follows: find $\mathbf{u} = \mathbf{u}(\rho) \in \boldsymbol{\mathcal{V}}_d$ such that

$$a(\rho; \mathbf{u}, \mathbf{v}) = 0 \quad \forall \mathbf{v} \in \boldsymbol{\mathcal{V}}_0. \tag{6}$$

Thanks to the choice of $\alpha(\rho)$, it turns out that the solution $\mathbf{u}$ of the above problem is (almost) null where $\rho = \rho_{\min}$ and solves a plane flow model where $\rho = 1$ (see [37] for more details). This amounts to interpret the region where $\rho = \rho_{\min}$ as occupied by a solid material, whereas the region where $\rho = 1$ as occupied by the fluid.

In order to formulate our optimization problem, let us introduce the energy functional $\mathcal{E}(\rho, \mathbf{u}) = \frac{1}{2}a(\rho; \mathbf{u}, \mathbf{u})$ which is a measure of the dissipated energy associated the pair $(\rho, \mathbf{u})$. Thus, the optimal flow problem governed by the Stokes equation reads as

$$\begin{cases} \min\limits_{\rho\in\mathcal{Q}_{\text{ad}}} & \mathcal{E}(\rho, \mathbf{u}) \\ \text{s.t.} & a(\rho; \mathbf{u}, \mathbf{v}) = 0 \quad \forall \mathbf{v} \in \boldsymbol{\mathcal{V}}_0 \\ & \dfrac{1}{V}\displaystyle\int_\Omega \rho dx \ \le V_f. \end{cases} \tag{7}$$

3. VEM discretization

In this section we briefly introduce the virtual element discretization of the topology optimization problems (4) and (7), which will be addressed in Sections 3.1 and 3.2, respectively. It is beyond the scope of the paper to give a detailed introduction and description of the Virtual Element Method (suitable pointers to the specific literature will be provided during the subsequent brief presentation). However, for the ease of reading, it is worth to highlight the main idea of VEM, namely that the explicit knowledge of the analytic expression of the VEM basis functions on each polygon is not needed.

Please cite this article in press as: P.F. Antonietti, et al., On the virtual element method for topology optimization on polygonal meshes: A numerical study, Computers and Mathematics with Applications (2017), http://dx.doi.org/10.1016/j.camwa.2017.05.025.

Indeed, the only crucial information required to assemble the VEM discrete problem is the knowledge of the basis functions at a suitable (unisolvent) set of degrees of freedom (together with an accurate strategy to approximate the right-hand side).

Let $\mathcal{T}_h$ represent a decomposition of Ω into general, possibly non-convex, polygonal elements E with $\mathrm{diam}(E) = h_E$, where $\mathrm{diam}(E) = \max_{x,y\in E}\|x-y\|$. In the following, we will denote by e the straight edges of the mesh $\mathcal{T}_h$ and, for all $e \in \partial E$, $\mathbf{n}_E^e$ will denote the unit normal vector to e pointing outward to E. We will use the symbol $\mathbb{P}_k(\omega)$ to denote the space of polynomials of degree less than or equal to $k \geq 1$ living on the set $\omega \subseteq \mathbb{R}^2$. Moreover, we will work under the following mesh regularity assumption on $\mathcal{T}_h$ (see, e.g., [3]):

Assumption 3.1. We assume that there exist positive constants c_s and c_s' such that every element $E \in \{\Omega_h\}_h$ is star shaped with respect to a ball with radius $\rho \geq c_s h_E$ and every edge $e \in \partial E$ has at least length $h_e \geq c_s' h_E$.

Let us first introduce the discrete counterpart of the space $\mathcal{Q}_{\mathrm{ad}}$, namely the finite dimensional space of piecewise constant admissible controls

$$\mathbb{Q}_{\mathrm{ad}} = \{\rho_h \in \mathcal{Q}_{\mathrm{ad}} : \ \rho_{h|E} \in \mathbb{P}_0(E) \ \forall E \in \mathcal{T}_h\}.$$

Clearly, a function $\rho_h \in \mathbb{Q}_{\mathrm{ad}}$ is uniquely determined by its value ρ_E in each polygon $E \in \mathcal{T}_h$. Hence, the dimension of $\mathbb{Q}_{\mathrm{ad}}$ equals the cardinality of $\mathcal{T}_h$.

3.1. Minimum compliance

Following [8], it is possible to introduce the low-order discrete VEM spaces $\mathbf{V}_{0,h} \subset \mathcal{V}_0$ and $\mathbf{V}_h \subset \mathcal{V}$, a discrete form $a_h(\rho_h; \mathbf{u}_h, \mathbf{v}_h)$ approximating $a(\rho; \mathbf{u}, \mathbf{v})$ and a discrete functional $\mathcal{F}_h(\mathbf{v}_h)$ approximating $\mathcal{F}(\mathbf{v})$ such that the VEM discretization of (3) reads as: given $\rho_h \in \mathbb{Q}_{\mathrm{ad}}$ find $\mathbf{u}_h \in \mathcal{V}_h$ such that

$$a_h(\rho_h; \mathbf{u}_h, \mathbf{v}_h) = \mathcal{F}_h(\mathbf{v}_h) \tag{8}$$

for any $\mathbf{v}_h \in \mathcal{V}_{0,h}$. In particular, the global VEM spaces $\mathbf{V}_{0,h}$ and $\mathbf{V}_h$ are obtained by gluing suitable local discrete VEM spaces, denoted by $\mathcal{V}_h(E)$, whose elements are uniquely identified by the values at the vertices of the polygon E and contain linear polynomials, i.e $(\mathbb{P}_1(E))^2 \subset \mathcal{V}_h(E)$. In passing, it is worth noticing that the presence of the linear polynomials in the VEM space dictates the order of accuracy of the resulting approximation of the differential problem. It is immediate to verify that the dimension of $\mathbf{V}_{0,h}$ (the same happens for $\mathbf{V}_h$) equals two times the number of the interior vertices of the partition $\mathcal{T}_h$ plus those belonging to Γ_t, having fixed the values at vertices belonging to Γ_d to incorporate Dirichlet boundary conditions. More precisely, according to [8], we have

$$\mathcal{V}_h(E) = \{\mathbf{v}_h \in (H^1(E))^2 : A_{\lambda_0,\mu_0}\mathbf{v}_h = \mathbf{0} \text{ on } E, \mathbf{v}_h|_e \in (\mathbb{P}_1(e))^2 \ \forall e \in \partial E\}$$

where

$$A_{\lambda_0,\mu_0}\mathbf{u} = -\begin{pmatrix} 2\mu_0\left(u_{1,xx} + \frac{1}{2}(u_{1,yy} + u_{2,xy})\right) + \lambda_0(u_{1,xx} + u_{2,yx}) \\ 2\mu_0\left(\frac{1}{2}(u_{1,yx} + u_{2,xx}) + u_{2,yy}\right) + \lambda_0(u_{1,xy} + u_{2,yy}) \end{pmatrix}.$$

Let us now define the projection operator $\Pi_E^\epsilon : \mathcal{V}_h(E) \to (\mathbb{P}_1(E))^2$ solution of

$$\begin{cases} a^E(\Pi_E^\epsilon \mathbf{v}_h, \mathbf{q}) = a^E(\mathbf{v}_h, \mathbf{q}) \quad \forall \mathbf{q} \in (\mathbb{P}_1(E))^2 \\ \overline{\Pi_E^\epsilon \mathbf{v}_h} = \overline{\mathbf{v}_h} \\ avr(\Pi_E^\epsilon \mathbf{v}_h) = avr(\mathbf{v}_h), \end{cases} \tag{9}$$

for all $\mathbf{v}_h \in \mathcal{V}_h(E)$, where $a^E(\cdot,\cdot)$ is the bilinear form $a(\cdot,\cdot)$ restricted to the element E and, for any regular function $\phi = (\phi_1, \phi_2)$, we set

$$\overline{\phi} = \left(\frac{1}{n}\sum_{i=1}^n \phi_1(V_i), \frac{1}{n}\sum_{i=1}^n \phi_2(V_i)\right)$$

and

$$avr(\phi) = \frac{1}{n}\sum_{i=1}^n [(y_i - y_b)\phi_1(V_i) + (-x_i + x_b)\phi_2(V_i)],$$

with $V_i = (x_i, y_i)$, $i = 1, \ldots, n$, and (x_b, y_b) vertices and barycenter of E, respectively. It is easy to see that Π_E^ϵ is computable from the degrees of freedom of the local VEM space.

As customary in the theory of VEM, the construction of the global form $a_h(\rho_h; \mathbf{u}_h, \mathbf{v}_h)$ hinges upon the construction of local forms $a_h^E(\mathbf{u}_h, \mathbf{v}_h) : \mathcal{V}_h(E) \times \mathcal{V}_h(E) \to \mathbb{R}$ defined as

$$a_h^E(\mathbf{u}_h, \mathbf{v}_h) = 2\mu_0 \int_E \epsilon(\Pi_E^\epsilon \mathbf{u}_h) : \epsilon(\Pi_E^\epsilon \mathbf{v}_h)\, d\mathbf{x} + \lambda_0 \int_E \mathrm{div}\, \Pi_E^\epsilon \mathbf{u}_h \,\mathrm{div}\, \Pi_E^\epsilon \mathbf{v}_h\, d\mathbf{x} + S^{E,\epsilon}(\mathbf{u}_h - \Pi_E^\epsilon \mathbf{u}_h, \mathbf{v}_h - \Pi_E^\epsilon \mathbf{v}_h),$$

Please cite this article in press as: P.F. Antonietti, et al., On the virtual element method for topology optimization on polygonal meshes: A numerical study, Computers and Mathematics with Applications (2017), http://dx.doi.org/10.1016/j.camwa.2017.05.025.

where the bilinear form $S^{E,\epsilon}$ is a suitable stabilization term with the same scaling properties of the sum of the first and second term (see [8] for more details). Then, the global form reads as follows:

$$a_h(\rho_h; \mathbf{u}_h, \mathbf{v}_h) = \sum_{E\in\mathcal{T}_h} \rho_E^p a_h^E(\mathbf{u}_h, \mathbf{v}_h), \tag{10}$$

where we employed the fact that $\rho_h|_E \in \mathbb{P}_0(E)$.

In the case of nearly-incompressible materials, i.e. for $\lambda_0 \to +\infty$, the local discrete bilinear form is modified as follows:

$$a_h^E(\mathbf{u}_h, \mathbf{v}_h) = 2\mu_0 \int_E \epsilon(\Pi_E^\epsilon \mathbf{u}_h) : \epsilon(\Pi_E^\epsilon \mathbf{v}_h)\, dx + \lambda_0 \int_E (\Pi_E^0 \mathrm{div}\mathbf{u}_h)(\Pi_E^0 \mathrm{div}\mathbf{v}_h)\, dx + S^{E,\epsilon}(\mathbf{u}_h - \Pi_E^\epsilon \mathbf{u}_h, \mathbf{v}_h - \Pi_E^\epsilon \mathbf{v}_h), \tag{11}$$

where Π_E^0 denotes the L^2-projection on constant functions and the bilinear form $S^{E,\epsilon}$ is a suitable stabilization term with the same scaling properties of the first term. We refer to [8] for more details.

Remark 3.1. By testing with $\mathbf{q} = (x, y)$ in Eq. (9), it is easy to see that, in the lowest order case considered here, it holds $\mathrm{div}\, \Pi_E^\epsilon \mathbf{v}_h = \Pi_E^0 \mathrm{div}\mathbf{v}_h$.

Remark 3.2. For nearly-incompressible elasticity, in [8] it is not theoretically proved that the resulting lowest-order discrete VEM problem stemming from (11) is well posed. However, in [38], it is proved that, in the context of Mimetic Finite Differences (MFD), the formulation is well posed on hexagons.

According to the previous considerations, the VEM discretization of the topology optimization problem (4) reads as follows:

$$\begin{cases} \min\limits_{\rho_h\in\mathbb{Q}_{\mathrm{ad}}} & \mathcal{C}(\rho_h, \mathbf{u}_h) = \mathcal{F}_h(\mathbf{u}_h) \\ \text{s.t.} & a_h(\rho_h; \mathbf{u}_h, \mathbf{v}_h) = \mathcal{F}_h(\mathbf{v}_h) \quad \forall \mathbf{v}_h \in \boldsymbol{\mathcal{V}}_{0,h} \\ & \dfrac{1}{V}\displaystyle\int_\Omega \rho_h dx \ \le V_f. \end{cases} \tag{12}$$

3.2. Optimal Stokes flow

Hinging upon the results of the previous sections, the virtual discretization of (7) easily follows. Indeed, bearing in mind (11), the discrete virtual counterpart of (6) reads as: given $\rho_h \in \mathbb{Q}_{\mathrm{ad}}$ find $\mathbf{u}_h \in \mathcal{V}_h$ such that

$$a_h(\rho_h; \mathbf{u}_h, \mathbf{v}_h) = \mathbf{0} \tag{13}$$

for any $\mathbf{v}_h \in \mathcal{V}_{0,h}$, where as usual the global discrete form $a_h(\rho_h; \mathbf{u}_h, \mathbf{v}_h)$ is defined in terms of the local forms as $a_h(\rho_h; \mathbf{u}_h, \mathbf{v}_h) = \sum_{E\in\mathcal{T}_h} a_h^E(\mathbf{u}_h, \mathbf{v}_h) + b_h^E(\rho_h; \mathbf{u}_h, \mathbf{v}_h)$ with $a_h^E(\mathbf{u}_h, \mathbf{v}_h)$ being the same as in (11) and

$$b_h^E(\rho_h; \mathbf{u}_h, \mathbf{v}_h) = \int_E \frac{5\mu_0}{\rho_E^2} \Pi_E^0 \mathbf{u}_h \cdot \Pi_E^0 \mathbf{v}_h dx + S^{E,0}(\mathbf{u}_h - \Pi_E^0 \mathbf{u}_h, \mathbf{v}_h - \Pi_E^0 \mathbf{v}_h), \tag{14}$$

where $\Pi_E^0 : \mathcal{V}_h(E) \to (\mathbb{P}_1(E))^2$ is the L^2-projection and the bilinear form $S^{E,0}$, as above, is a suitable stabilization term with the same scaling properties of the first term. Note that, using the *augmented space argument* (see [39]), on the local VEM space the projections Π_E^0 and Π_E^ϵ coincide, thus Π_E^0 is computable.

In order to formulate the discrete optimization problem, let us introduce the energy functional $\mathcal{E}_h(\rho_h, \mathbf{u}_h) = \frac{1}{2} a_h(\rho; \mathbf{u}_h, \mathbf{u}_h)$. Thus, the virtual discretization of (7) reads as

$$\begin{cases} \min\limits_{\rho\in\mathbb{Q}_{\mathrm{ad}}} & \mathcal{E}(\rho_h, \mathbf{u}_h) \\ \text{s.t.} & a(\rho_h; \mathbf{u}_h, \mathbf{v}_h) = 0 \quad \forall \mathbf{v}_h \in \boldsymbol{\mathcal{V}}_{0,h} \\ & \dfrac{1}{V}\displaystyle\int_\Omega \rho_h dx \ \le V_f. \end{cases} \tag{15}$$

4. Numerical results

Several numerical examples are presented in this section dealing with the VEM discretization of the topology optimization problems introduced above. The minimum compliance problem governed by compressible (Section 4.1) and nearly-incompressible linear elasticity (Section 4.2) is solved, as well as the optimal flow problem governed by the Stokes equation (Section 4.3).

The Method of Moving Asymptotes (MMA) [40], an algorithm based on sequential convex programming, is herein adopted to tackle the discrete optimization problems (12)–(15).

Please cite this article in press as: P.F. Antonietti, et al., On the virtual element method for topology optimization on polygonal meshes: A numerical study, Computers and Mathematics with Applications (2017), http://dx.doi.org/10.1016/j.camwa.2017.05.025.

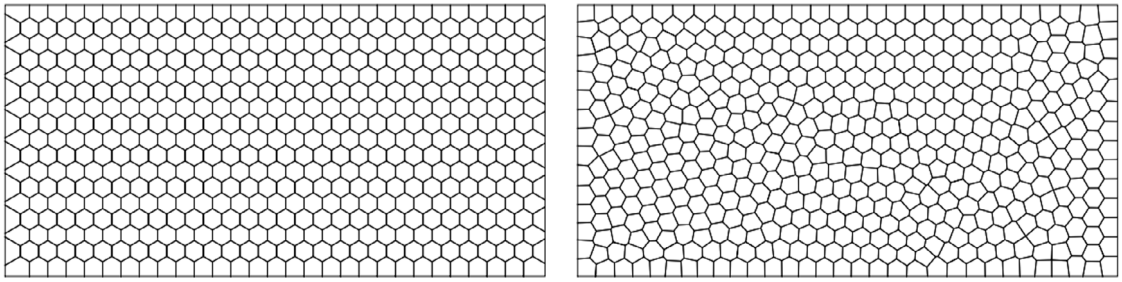

Fig. 1. Examples of structured (left) and unstructured (right) polygonal grids consisting of 501 elements.

As described in the previous section, an element-wise density discretization is implemented to approximate the unknown density field.

When addressing elasticity, this conventional discrete scheme can be affected by undesired numerical instabilities, such as checkerboard patterns and mesh dependence, see e.g. [41]. The former issue arises depending on the shape functions adopted to discretize the displacement field and solve the elastic problem; the latter arises as the discrete counterpart of a lack of well-posedness of the continuum problem of topology optimization. Four-node (displacement-based) finite elements are well-known to be affected by checkerboard patterns, whereas polygonal elements have been found to be free from such an issue [32]. On both kinds of discretizations, the achieved optimal layouts suffer from mesh-dependence.

Several methods are available in the literature to overcome the numerical instabilities above mentioned [42]. Following [43] and some robust application in stress-constrained topology optimization, see e.g. [44–47], a filter is herein applied to the density unknowns ρ_E and a new set of physical variables $\tilde{\rho}_E$ is defined as:

$$\tilde{\rho}_E = \frac{1}{\sum_{E' \in \mathcal{T}_h} H_{E,E'}} \sum_{E' \in \mathcal{T}_h} H_{E,E'} \rho_{E'}, \quad H_{E,E'} = V'_E \max(0, r_{\min} - \mathrm{dist}(E, E')). \tag{16}$$

In the above equation $\mathrm{dist}(E, E')$ is the distance between the centroid of the elements E and E', whereas V'_E, the volume of the element E', is taken into account to improve results on irregular meshes; $r_{\min} > d_m$ is the size of the filter radius; d_m is the average square root of the area of the polygons/elements in the discretization $\mathcal{T}_h$. Enforcing $r_{\min} = 1, 5d_m$, undesired checkerboard patterns are inhibited; adopting larger values of $r_{\min}$ a heuristic control on the minimum thickness of any member in the design is additionally embedded within the optimization.

In the sequel, this filtering technique will be applied to problems of optimal design involving elasticity, both for the FEM-based and the VEM-based approach. We note that, differently from the elasticity case where the filtering technique is essential to prove existence of solutions and to avoid numerical instabilities (see e.g. [48]), the optimal Stokes flow problems will be tackled without introducing any regularization approach, since the continuous problem is well-posed and no numerical instability is expected, see [37].

4.1. Compressible elasticity

In this section a set of numerical simulations is performed to investigate the features of the proposed VEM-based procedure when addressing topology optimization governed by compressible elasticity. Structured and Central Voronoi Tessellation (CVT) polygonal grids have been employed to discretize the design domain. In the following, we will denote by *unstructured* the CVT meshes. Fig. 1 shows examples of grids including 501 polygonal elements. The achieved VEM-based results are compared with analogous ones obtained by employing the classical bilinear finite elements on Cartesian meshes, see [41]. A linear elastic isotropic material is considered in the simulations, assuming Young modulus $E = 1$ and Poisson's ratio $\nu = 0.3$, if not differently specified. In the whole set of minimizations, the volume fraction of available material is $V_f = 0.3$. Different values of filter radius are considered.

A set of preliminary numerical simulations is performed on the square lamina represented in Fig. 2. The specimen is clamped along the whole left side, whereas $P = 2$ is the intensity of the horizontal traction applied at the central node of the right side. The black region stands for a rigid non-design zone, whose aim is distributing the point load to the whole right side. Due to the symmetry of geometry and boundary conditions, only the bottom half of the domain has been tackled in the optimization: traction has been halved whereas vertical displacements have been enforced to be null along the symmetry axis. Zero Poisson's ratio is considered for the material all over the domain. In case of a perfectly rigid non-design region, multiple solutions are expected, consisting of one or more straight bars. All of them are equally efficient in terms of compliance.

A structured mesh made of 2006 polygonal elements (2^5 elements lie along the thickness of the lamina) is used to perform the numerical simulations, enforcing a stiff non-design region whose Young modulus is 10^3 times that of the elastic material elsewhere. The proposed VEM-based minimization algorithm is tested without density filter. As expected, adopting different

Please cite this article in press as: P.F. Antonietti, et al., On the virtual element method for topology optimization on polygonal meshes: A numerical study, Computers and Mathematics with Applications (2017), http://dx.doi.org/10.1016/j.camwa.2017.05.025.

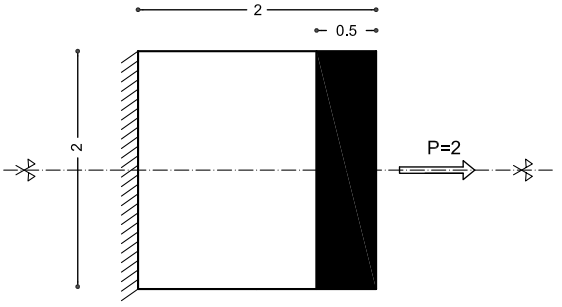

Fig. 2. Compressible elasticity with zero Poisson's ratio. Geometry and boundary conditions for a square lamina. $P = 2$ is the resultant of the horizontal traction applied as a nodal force.

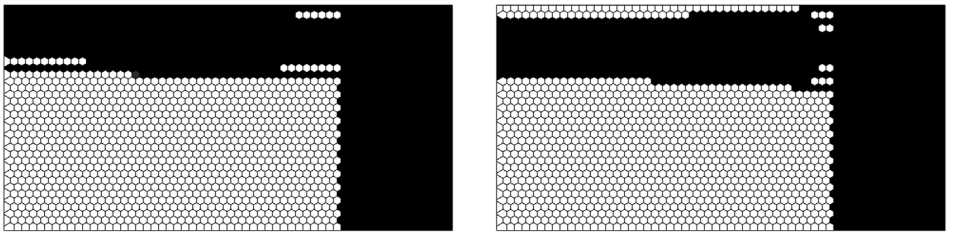

Fig. 3. Compressible elasticity with zero Poisson's ratio. Optimal design achieved with no density filter, assuming as a starting guess: $\rho_E = V_f$ all over the domain (left) and $\rho_E = 1$ all over the domain (right).

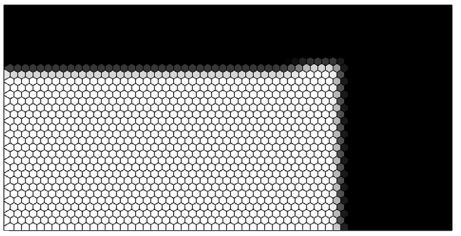

Fig. 4. Compressible elasticity with zero Poisson's ratio. Optimal design achieved with density filter.

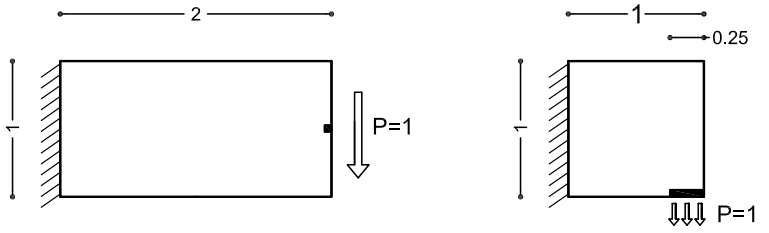

Fig. 5. Compressible elasticity. Geometry and boundary conditions for the numerical simulations of Example 1 (rectangular cantilever, left) and Example 2 (square cantilever, right). In each case $P = 1$ is the resultant of the traction $\mathbf{f}_t$ oriented as indicated by the arrow. The load is applied as a nodal force in Example 1 and as a traction along a prescribed boundary in Example 2.

starting guesses, multiple crisp 0–1 solutions are found with approximately the same compliance. Fig. 3 shows the optimal layouts found assuming, as a starting guess, a uniform distribution with $\rho_E = V_f$ (left) and $\rho_E = 1$ (right). No checkerboard pattern or point-to-point connection arises, as originally investigated by [32]. Branching of the design can be limited through the implementation of the filtering approach presented above. Fig. 4 shows the optimal design that can been found for $r_{\min} = 3.0 d_m$, initializing the density field for both starting guesses mentioned above.

4.1.1. Example 1: rectangular cantilever

The first design problem refers to the rectangular cantilever represented in Fig. 5(left). A reference solution is conventionally obtained implementing bilinear finite elements on a Cartesian grid consisting of 8192 squares (2^6 elements lie along

Please cite this article in press as: P.F. Antonietti, et al., On the virtual element method for topology optimization on polygonal meshes: A numerical study, Computers and Mathematics with Applications (2017), http://dx.doi.org/10.1016/j.camwa.2017.05.025.

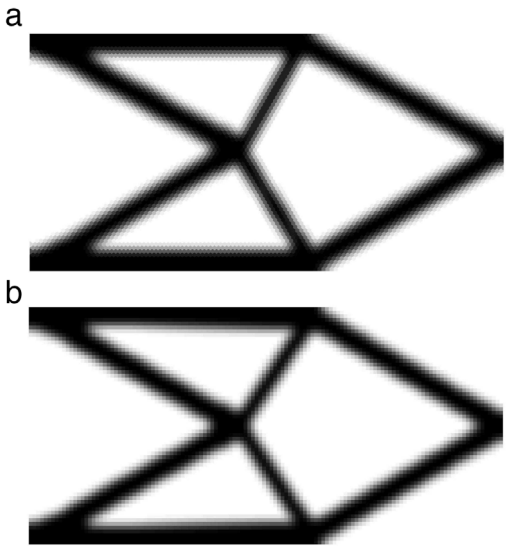

Fig. 6. Compressible elasticity. Example 1: rectangular cantilever. Optimal topologies computed on structured meshes with 2^6 elements along the thickness of the cantilever: proposed VEM-based formulation (a), bilinear FEM-based formulation (b).

the thickness of the cantilever), along with a filter radius $r_{\min} = 3.0d_m$. As shown in Fig. 6(b), a truss-like structure arises: inclined members carry shear forces whereas horizontal ones cope with bending actions; both set of members undergo axial stresses. Fig. 6(a) shows the optimal design found through the proposed VEM-based minimization algorithm on a structured mesh consisting of 7990 polygonal elements (2^6 elements lie along the thickness of the cantilever). The same filter radius is adopted, e.g. $r_{\min} = 3.0d_m$. The result obtained with our VEM-based method is substantially equal to the one found by the classical FEM-based approach. Fig. 7 shows the history plot of the objective function for the considered optimization procedures. Both algorithms are started adopting $\rho_E = V_f$ all over the domain and terminated when the relative difference between the values of each density unknowns in two subsequent iterations is less than 0.001. The VEM-based curve is as smooth as the FEM-based one, whereas the number of iterations needed by the former procedure to achieve convergence is slightly larger than for the latter.

An additional set of numerical simulations is performed on a coarser discretization adopting 2^5 elements along the thickness of the cantilever. The same filter radius implemented in the previous investigations is assumed. Fig. 8(a) shows the optimal layout found through the proposed VEM-based approach on a structured mesh consisting of 2006 polygonal elements, whereas Fig. 8(b) refers to the optimal design achieved by the bilinear FEM-based approach on a regular mesh of 2048 square elements. Although the main layout of Fig. 6 is recovered in both pictures, the FEM-based design is affected by an unexpected variation in the inclination of the thinner reinforcing braces. Due to the limited amount of available material ($V_f = 0.3$) and the rough mesh of square elements, the optimizer gets stuck in a final layout with 45-degree inclination, a mesh-dependent local minimum. The VEM-based result is not affected by such a numerical instability. Indeed, the VEM-based algorithm succeeds in finding the expected layout even in case of coarse unstructured meshes; Fig. 9 shows the optimal design obtained on a discretization consisting of 2048 unstructured polygonal elements for the same filter radius $r_{\min}$ as above. Fig. 10 shows the history plot of the objective function for the VEM-based optimization procedures whose results are presented in Figs. 8(a) and 9, sharing the same number of elements along the thickness of the cantilever (2^5). Both curves (structured and unstructured mesh) are smooth and converge to the same optimal value. With respect to the structured mesh, the unstructured one calls for a slightly increased number of iterations to find the final plateau and achieve convergence.

Fig. 11 provides a comparison between the VEM-based approach (see Fig. 11(a)) and the FEM-based one (see Fig. 11(b)) for fine regular meshes of 32 028 and 32 768 elements, respectively (2^7 elements lie along the thickness of the cantilever). Notwithstanding the adopted smaller filter radius $r_{\min} = 1.5d_m$, the achieved optimal layouts are almost identical.

4.1.2. Example 2: square cantilever

The second investigation addresses the square cantilever shown in Fig. 5(right). An assessment of the VEM-based topology optimization method is provided, adopting unstructured grids of polygonal elements as those shown in Fig. 1(b).

First, an unstructured discretization accounting for 4096 elements (2^6 along the thickness of the cantilever) is used. The adopted filter radius reads $r_{\min} = 1.5d_m$, being d_m, as before, the square root of the average area of the polygonal elements in the unstructured grid. Fig. 12 shows the achieved optimal layout, a truss-like structure whose central node receives two thick tensile-stressed trusses along with two thin compressive-stressed bars. Fig. 13 shows the optimal solutions achieved

Please cite this article in press as: P.F. Antonietti, et al., On the virtual element method for topology optimization on polygonal meshes: A numerical study, Computers and Mathematics with Applications (2017), http://dx.doi.org/10.1016/j.camwa.2017.05.025.

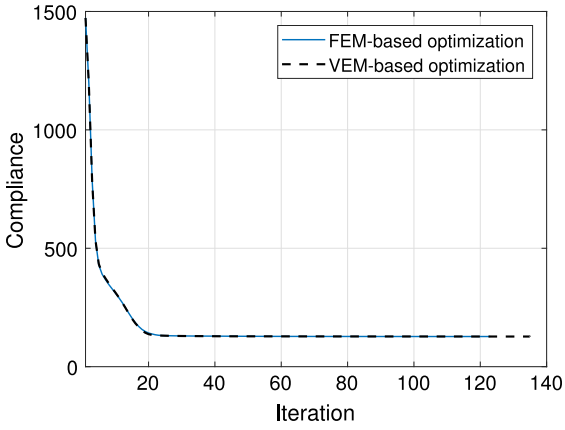

Fig. 7. Compressible elasticity. Example 1: rectangular cantilever. History plot of the objective function computed on structured meshes with 2^6 elements along the thickness of the cantilever: proposed VEM-based formulation vs. bilinear FEM-based formulation.

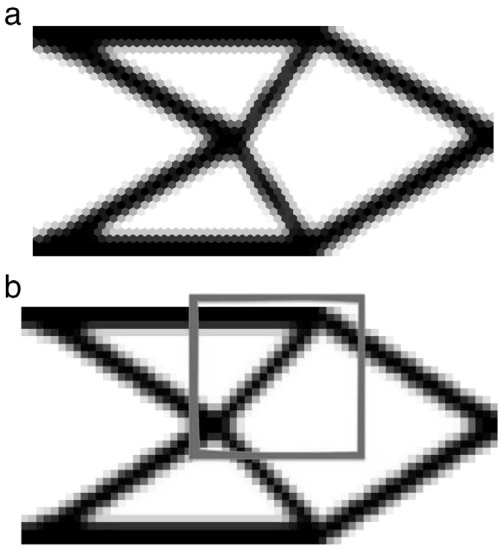

Fig. 8. Compressible elasticity. Example 1: rectangular cantilever. Optimal topologies computed on structured meshes with 2^5 elements along the thickness of the cantilever: proposed VEM-based formulation (a), bilinear FEM-based formulation (b).

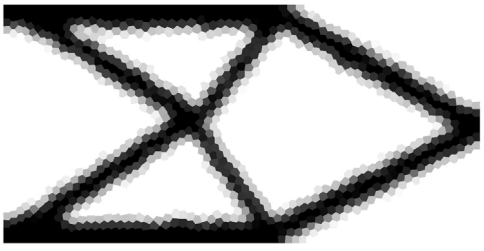

Fig. 9. Compressible elasticity. Example 1: rectangular cantilever. Optimal topology achieved through the proposed VEM-based formulation for an unstructured mesh with 2^5 elements along the thickness of the cantilever.

for an increased value of the enforced filter radius, i.e. $r_{\min} = 3.0d_m$. A simpler design arises that is made of two ties and one big strut, in full agreement with the well-known solution of this benchmark problem, see e.g. [41].

Finally, Fig. 14 provides the optimal layout computed when a finer discretization with 2^7 elements along the thickness of the cantilever is implemented. The overall number of polygonal elements is 16 384. The filter radius is $r_{\min} = 6.0d_m$, which is nearly the value used for the result shown in Fig. 13. No mesh dependence affects the proposed VEM-based formulation, since the same optimal layout is found in both figures.

Please cite this article in press as: P.F. Antonietti, et al., On the virtual element method for topology optimization on polygonal meshes: A numerical study, Computers and Mathematics with Applications (2017), http://dx.doi.org/10.1016/j.camwa.2017.05.025.

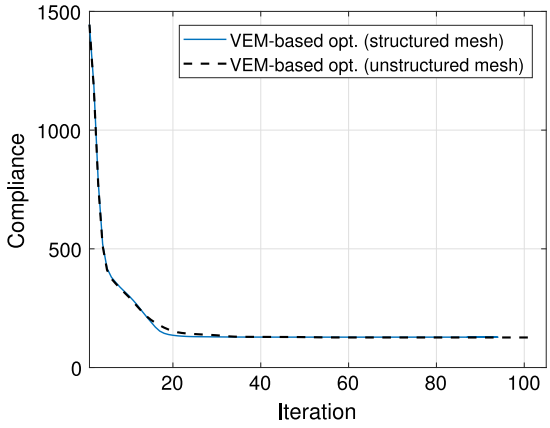

Fig. 10. Compressible elasticity. Example 1: rectangular cantilever. History plot of the objective function computed on meshes with 2^5 elements along the thickness of the cantilever for the proposed VEM-based formulation: structured vs. unstructured mesh.

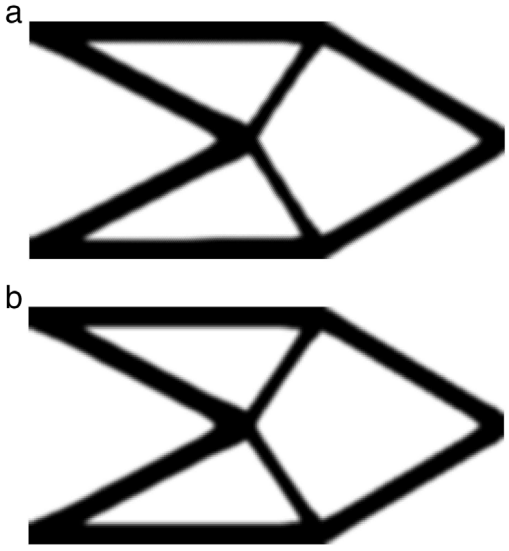

Fig. 11. Compressible elasticity. Example 1: rectangular cantilever. Optimal topologies computed on structured meshes with 2^7 elements along the thickness of the cantilever: proposed VEM-based formulation (a), bilinear FEM-based formulation (b).

4.1.3. Example 3: circle loaded with four point load

Let us consider a circular lamina that is loaded by a set of self-balanced forces applied at points A, B, C, D as shown in Fig. 15.

The geometry is discretized using a commercial code to achieve a mesh of 2168 quadrilateral elements, see Fig. 16. The conventional FEM-based formulation is adopted to find the volume-constrained minimum compliance solution. First, the load case presented in Fig. 15 is applied to the mesh in Fig. 16. Then, the same load case is applied to the discretization achieved after a 30-degree anticlockwise rotation of the original mesh around its centroid. This rotation has been chosen to investigate a mesh where the direction of the loads is not the same of the sides of (most of) the quadrilateral elements. Fig. 17 shows the result of the topology optimization procedure for the unrotated mesh of standard bilinear finite elements (see Fig. 17(a)) and the rotated one (see Fig. 17(b)). The achieved layouts are remarkably different and point out a lack of robustness of the solution with respect to the considered rotation of the mesh. In both cases a mesh-dependent solution is found that is not a truss-like structure. Due to the geometrical features of the adopted discretizations, non-straight members arise, curved beams in Fig. 18(a) or piecewise linear elements in Fig. 18(b). Both kinds of elements have to cope with bending stresses, meaning that a sub-optimal performance is achieved with respect to any stiff truss-like structure.

A similar investigation is performed adopting the proposed VEM-based approach to solve the considered problem of optimal design. The geometry is discretized using the academic code `Polymesher` [34] to achieve a mesh of 2268 polygonal elements, see Fig. 18. Fig. 19 shows the results of the VEM-based topology optimization for the unrotated mesh of Fig. 18(a) and for a discretization achieved after a 30-degree anticlockwise rotation of the original mesh around its centroid (b). The

Please cite this article in press as: P.F. Antonietti, et al., On the virtual element method for topology optimization on polygonal meshes: A numerical study, Computers and Mathematics with Applications (2017), http://dx.doi.org/10.1016/j.camwa.2017.05.025.

Fig. 12. Compressible elasticity. Example 2: square cantilever. Optimal topology computed with the proposed VEM-based formulation on an unstructured mesh with 2^6 elements along the thickness of the cantilever and filter radius $r_{\min} = 1.5d_m \approx 1.5/2^6$.

Fig. 13. Compressible elasticity. Example 2: square cantilever. Optimal topology computed with the proposed VEM-based formulation on an unstructured mesh with 2^6 elements along the thickness of the cantilever and filter radius $r_{\min} = 3.0d_m \approx 1.5/2^5$.

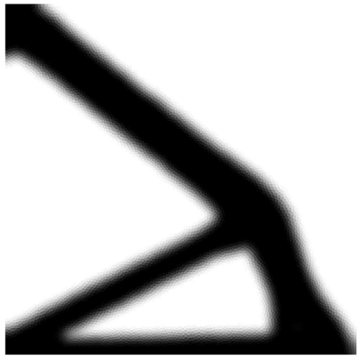

Fig. 14. Compressible elasticity. Example 2: square cantilever. Optimal topology computed with the proposed VEM-based formulation on an unstructured mesh with 2^7 elements along the thickness of the cantilever and filter radius $r_{\min} = 6.0d_m \approx 1.5/2^5$.

achieved layouts are very similar to each other: the considered rotation of the mesh induces only minor effects on the solution. In both cases a stiff truss-like structure arises, thus assessing the robustness of the proposed algorithm with respect to mesh rotations.

It must be remarked that the discretizations used for the optimal results in Figs. 17 and 19 share approximately the same number of elements (i.e. minimization unknowns), whereas the number of displacement degrees of freedom is different: 2×2245 dofs for the FEM-based discretization vs. 2×4525 dofs for the VEM-based discretization. Hence, an additional investigation is performed discretizing the circular geometry through the same commercial code used to find the mesh represented in Fig. 16, but aiming at an increased refinement. Fig. 20 shows the optimal design achieved on a mesh with 4116 quadrilateral elements along with 2×4225 displacement degrees of freedom. A 30-degree anticlockwise rotation is considered, as previously investigated in Fig. 17(b). Although the displacement dofs of this mesh are almost twice than

Please cite this article in press as: P.F. Antonietti, et al., On the virtual element method for topology optimization on polygonal meshes: A numerical study, Computers and Mathematics with Applications (2017), http://dx.doi.org/10.1016/j.camwa.2017.05.025.

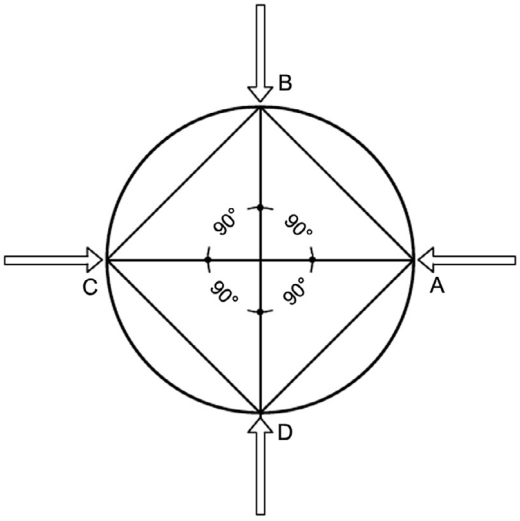

Fig. 15. Compressible elasticity. Geometry and boundary conditions for the numerical simulations of Example 3 (circle loaded with four point load).

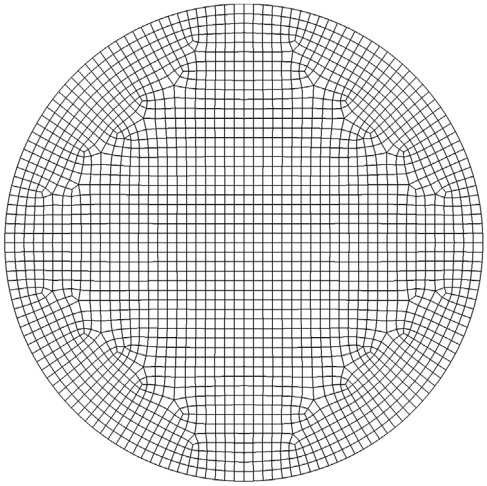

Fig. 16. Compressible elasticity. Example 3: circle loaded with four point load. Mesh of 2168 quadrilateral elements built with a commercial code,

for the VEM-based discretization shown in Fig. 18, the achieved results are not free from undesired effects induced by the geometrical features of the mesh (see e.g. the external straight members that are not perfectly aligned with the load application directions).

4.2. Nearly-incompressible elasticity

Differently from classical bilinear finite elements, the adopted VEM approximation is well-suited to cope with the analysis of quasi-incompressible media, since, at least on hexagons (see Remark 3.2), it satisfies the classical inf–sup stability condition and no locking is expected when dealing with problems assuming plane strain. As originally investigated in [49], a conventional SIMP-law that uses the same exponent p to approximate the dependence of the modulus λ and μ with respect to the density ρ can fail when addressing the optimal design of (nearly-)incompressible media: region with low density but high stiffness may arise in the solution, thus achieving optimal layouts that are unfeasible from a physical point of view. This problem can be simply overcome adopting a larger penalization on λ than μ, e.g. enforcing $p_\lambda = 6$ along with $p_\mu = 3$ instead of $p_\lambda = p_\mu = 3$, see [50].

Fig. 21(left) shows a benchmark problem for nearly-incompressible two-dimensional bodies undergoing plane strain conditions. A rectangular lamina is clamped along the bottom half of the vertical edges, whereas two point loads are applied in the middle of the extrados and of the intrados. Due to the symmetry of geometry and boundary conditions, only half of

Please cite this article in press as: P.F. Antonietti, et al., On the virtual element method for topology optimization on polygonal meshes: A numerical study, Computers and Mathematics with Applications (2017), http://dx.doi.org/10.1016/j.camwa.2017.05.025.

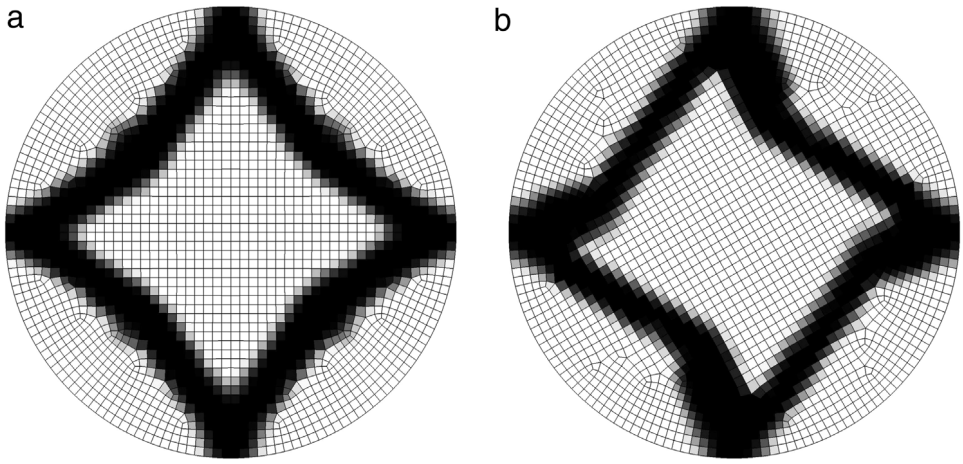

Fig. 17. Compressible elasticity. Example 3: circle loaded with four point load. Final configuration with bilinear FEM-based formulation: (a) no mesh rotation; (b) mesh rotation of 30°.

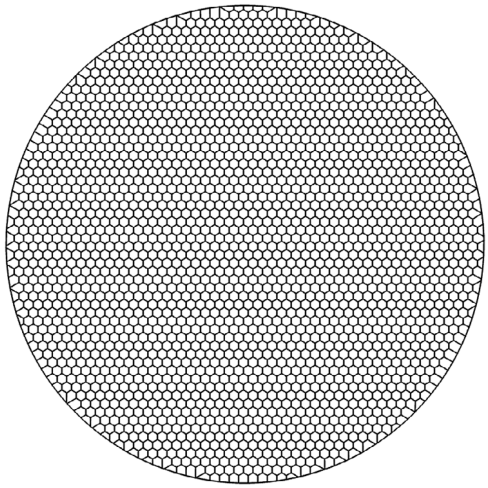

Fig. 18. Compressible elasticity. Example 3: circle loaded with four point load. Polygonal grid consisting of 2268 elements built with `Polymesher` [34].

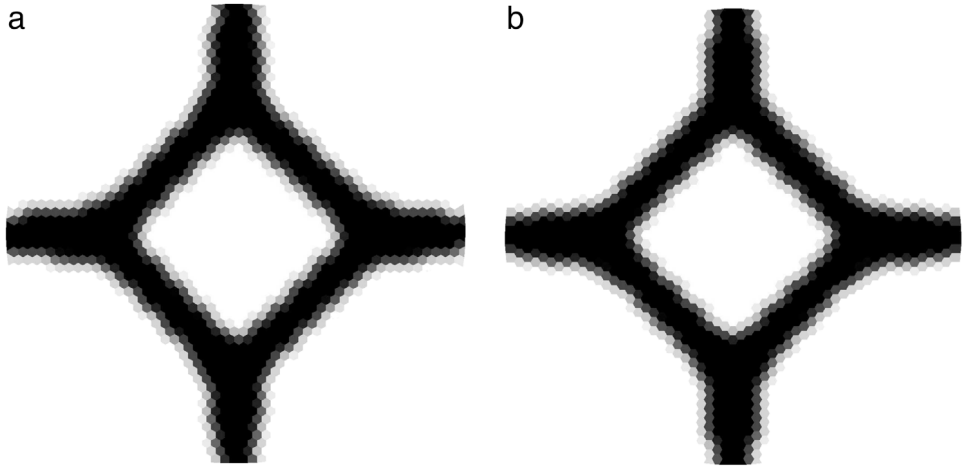

Fig. 19. Compressible elasticity. Example 3: circle loaded with four point load. Final configuration with VEM on structured meshes with 2268 elements: (a) no mesh rotation; (b) mesh rotation of 30°.

Please cite this article in press as: P.F. Antonietti, et al., On the virtual element method for topology optimization on polygonal meshes: A numerical study, Computers and Mathematics with Applications (2017), http://dx.doi.org/10.1016/j.camwa.2017.05.025.

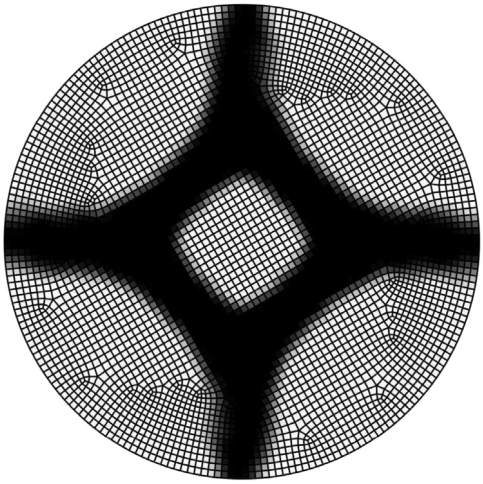

Fig. 20. Compressible elasticity. Example 3: circle loaded with four point load. Final configuration with bilinear FEM-based formulation and a discretization with 4116 elements: mesh rotation of 30°.

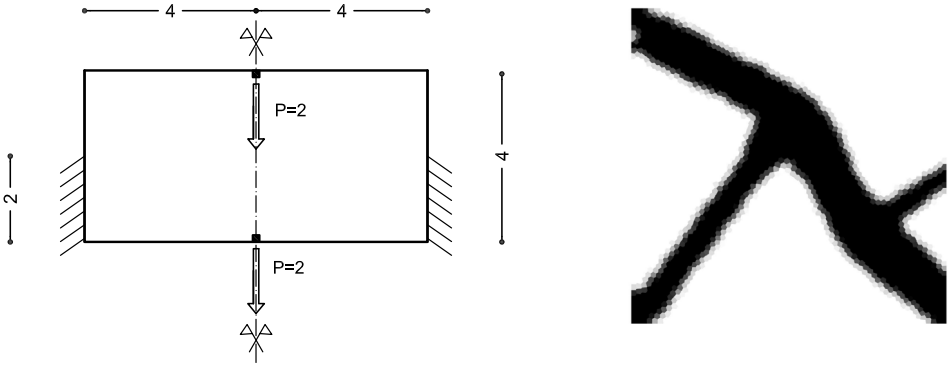

Fig. 21. Nearly-incompressible elasticity. Left: design domain. Right: optimal design (half by symmetry) on polygonal grid consisting of 4096 hexagons ($\nu = 0.4999999$).

the domain has been tackled in the optimization: loads have been halved and horizontal displacements have been enforced to be null along the symmetry axis. Fig. 21(right) shows the optimal design obtained by our VEM-based procedure on the right part of the original domain. The achieved layout is in full agreement with those found in the literature, see in particular the results obtained by adopting robust truly-mixed discretizations based on triangles [50] or square elements [51].

4.3. Optimal stokes flow

In this section we consider the numerical solution of the discrete problem (15) related to the optimization of Stokes flows. In particular, we will deal with some classical benchmark examples first introduced in [37] together with some suitable variants aiming at highlighting the virtues of the VEM-based topology optimization on polygonal meshes.

In the sequel, following [37] we will work under the following choice of the penalty function $\alpha(\rho)$ (cf. (5)), namely

$$\alpha(\rho) = \bar{\alpha} + (\underline{\alpha} - \bar{\alpha})\rho\frac{1+q}{\rho+q},$$

where $q = 0.1$, $\underline{\alpha} = 2.5\mu_0/100^2$ and $\bar{\alpha} = 2.5\mu_0/0.01^2$.

The profile of the prescribed non-zero velocity at the boundary is parabolic, i.e. the magnitude of the velocity can be written as $g^*(1-(2s/l)^2)$, with $s \in [-l/2, l/2]$ where g^* is the maximum value, whereas l is the length of the boundary part where the parabolic profile is prescribed.

Throughout all the following numerical experiments we choose $\mu_0 = 1$ and $\lambda_0 = 10^3$. We remark that, in view of the discussion at the beginning of this section, no filtering techniques are employed.

Please cite this article in press as: P.F. Antonietti, et al., On the virtual element method for topology optimization on polygonal meshes: A numerical study, Computers and Mathematics with Applications (2017), http://dx.doi.org/10.1016/j.camwa.2017.05.025.

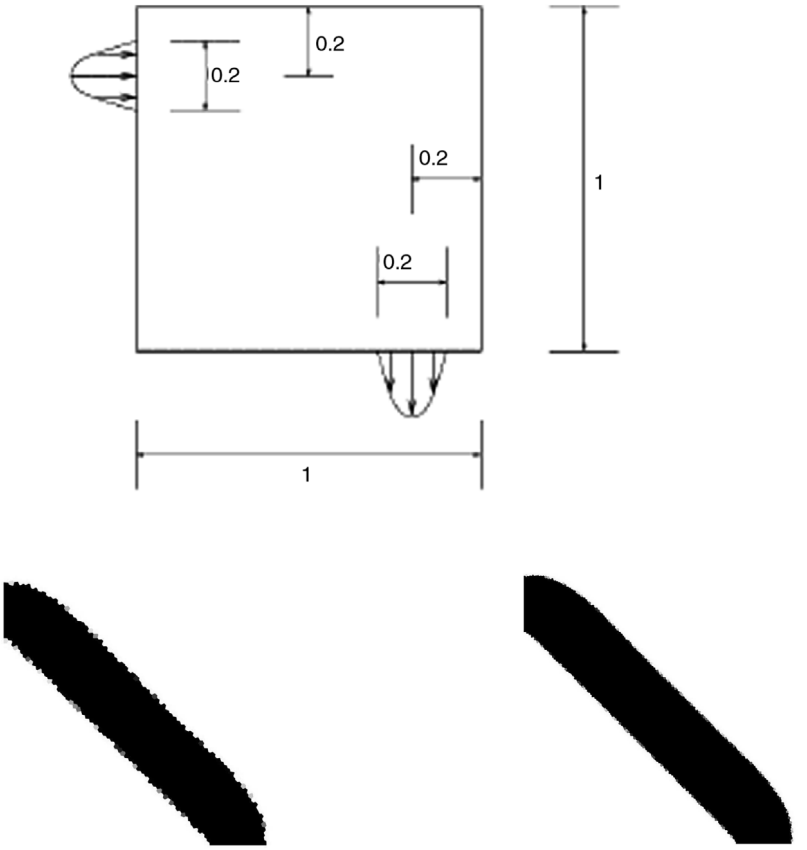

Fig. 22. Optimal pipe. Top: design domain (taken from [37]). Bottom: optimal configuration on unstructured polygonal grid consisting of 4096 (left) and 16 384 (right) elements.

4.3.1. Optimal pipe

Here we consider the design region depicted in Fig. 22(top) where the inflow equals the outflow and set $g^* = 1$. We employ an unstructured mesh of hexagons made of 4096 and 16 384 elements, respectively and the obtained optimal shapes of the pipe minimizing the dissipated energy are shown in Fig. 22(bottom). The optimal result is in agreement with the configuration found in the literature (see, e.g., [37]).

4.3.2. Optimal pipe with obstacle

In this section we modify the previous test case by including an obstacle represented by a circle centered at $C = (0.5, 0.5)$ with radius $r = 0.3$ (see Fig. 23(top)). Thus the circle is a non-design region, i.e. $\rho_h = \rho_{\min}$, and the optimal flow has to accommodate the presence of the obstacle. The results of the optimization process are reported in Fig. 23(bottom) and clearly show the capability of the polygonal mesh to accommodate curved no-design regions.

4.3.3. Optimal diffuser

Here we consider the design region depicted in Fig. 24 (top) where the inflow and the outflow have been chosen to respect the mass conservation, i.e. $g^* = 1$ at the inlet and $g^* = 3$ at the outlet. We employ an unstructured mesh of hexagons made of 4096 and 16 384 elements, respectively, and the obtained optimal shape of the pipe minimizing the dissipated energy is shown in Fig. 24 (bottom). Also in this case, the optimal result obtained with our VEM based approach is in agreement with the configuration found in the literature (see, e.g., [37]).

4.3.4. Optimal diffuser with obstacle

Similarly to the optimal pipe test, we modify the previous test case by including a circular obstacle ($\rho_h = \rho_{\min}$) centered at $C = (0.5, 0.5)$ with radius $r = 0.1$ (see Fig. 25(top)). The optimal flow taking into account the presence of the obstacle is reported in Fig. 25(bottom) for two polygonal grids with 4096 and 16 384 elements, respectively. The same comments of Section 4.3.2 apply here.

Please cite this article in press as: P.F. Antonietti, et al., On the virtual element method for topology optimization on polygonal meshes: A numerical study, Computers and Mathematics with Applications (2017), http://dx.doi.org/10.1016/j.camwa.2017.05.025.

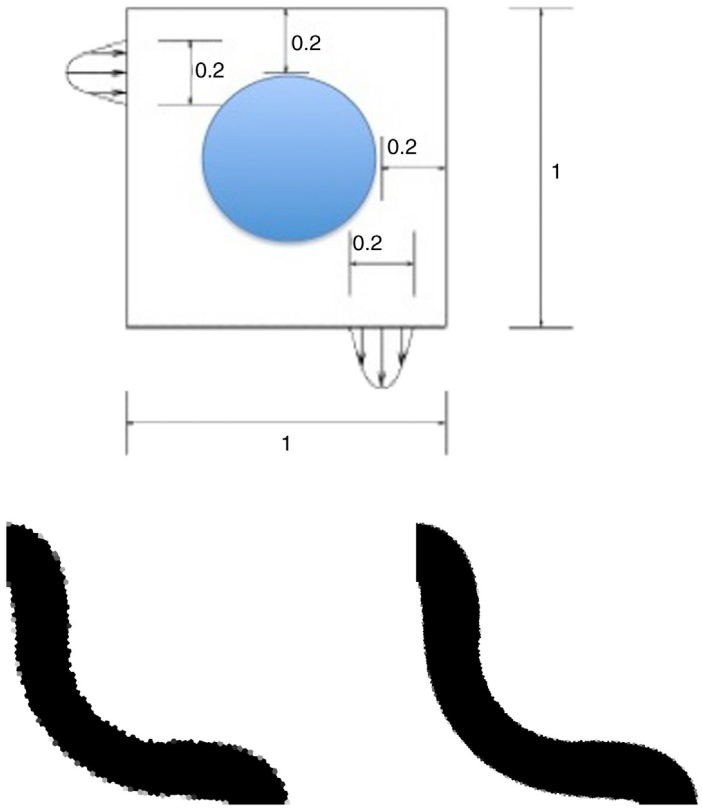

Fig. 23. Optimal pipe with obstacle. Top: design domain with circular obstacle. Bottom: optimal configuration on unstructured polygonal grid consisting of 4096 (left) and 16 384 (right) elements.

5. Conclusions

In this paper we considered the numerical solution of two paradigmatic examples of topology optimization problems on polygonal meshes employing the virtual element method. The first optimization problem is the minimum compliance governed by linear elasticity (compressible and nearly-incompressible) while the second one is related to the minimum energy dissipation of Stokes flows. From the numerical results presented in the previous section, we can draw the following conclusions:

- optimal layouts do not seem to be affected by the geometrical features of the polygonal mesh, whereas the use of standard quadrilateral grids may steer the optimization process towards sub-optimal (non-physical) configurations;
- optimal layouts obtained with polygonal meshes seem to be more robust with respect to mesh rotations, whereas rotated standard quadrilateral grids may give rise to different optimal configurations;
- optimal configurations obtained on polygonal meshes seem to be mesh independent, i.e. they do not seem to depend on the granularity of the computational mesh;
- optimal layouts in the case of topology optimization governed by nearly-incompressible elasticity or Stokes flow have been successfully identified, thanks to the accuracy and stability properties of the adopted virtual element approximation.

Hinging on the results of the present paper, it seems to be promising, in terms of reduction of the overall computational cost, the adoption of mesh adaptivity during the optimization process (see, e.g., [52,53]). Moreover, the outcome of this work could be of interest for topology optimization in fluid–structure interaction problems (see, e.g. [54]). These topics will be addressed in future works.

Acknowledgment

The authors wish to thank Prof. Ole Sigmund for suggesting the adoption of a version of the density filter depending on the element volume to improve results in case of irregular meshes.

Please cite this article in press as: P.F. Antonietti, et al., On the virtual element method for topology optimization on polygonal meshes: A numerical study, Computers and Mathematics with Applications (2017), http://dx.doi.org/10.1016/j.camwa.2017.05.025.

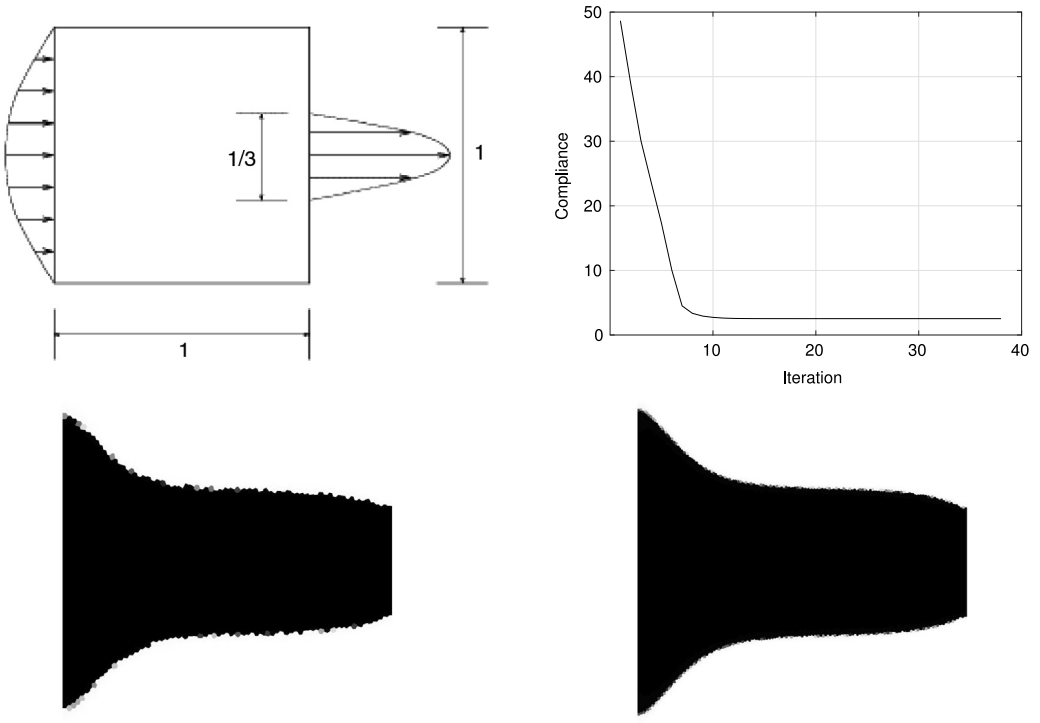

Fig. 24. Optimal diffuser. Top: design domain (left) and history plot (right) of the objective function computed from the case of 16 384 elements below. Bottom: optimal configuration on unstructured polygonal grid consisting of 4096 (left) and 16 384 (right) elements.

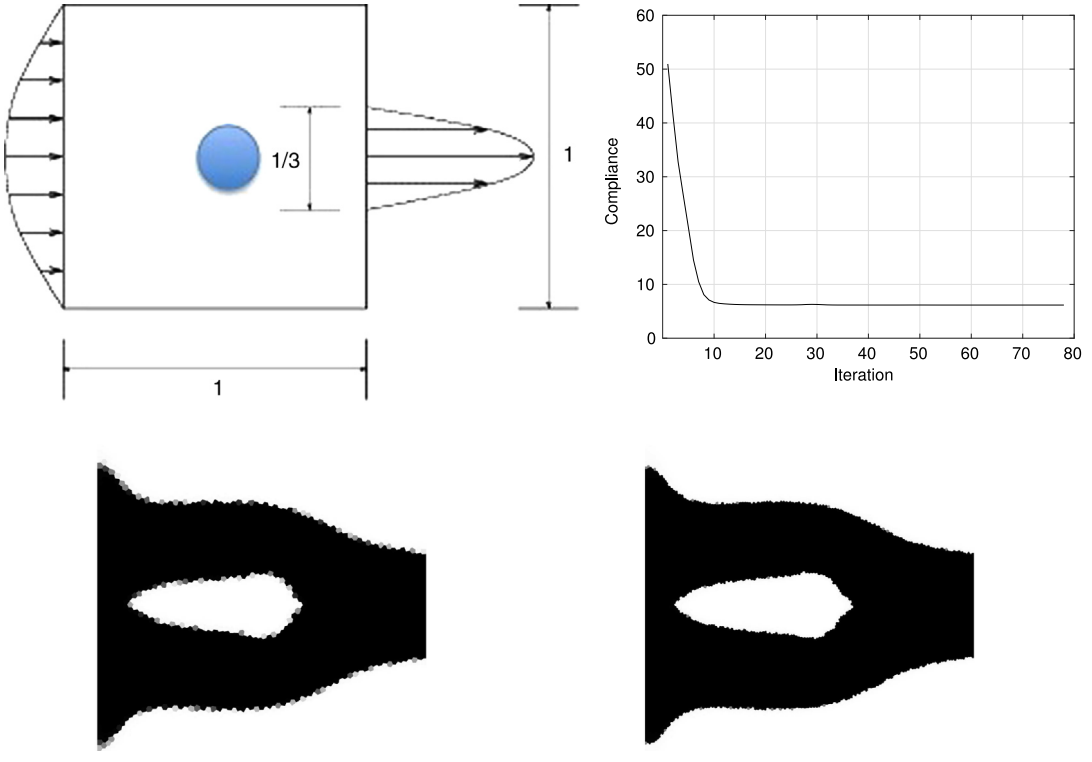

Fig. 25. Optimal diffuser with obstacle. Top: design domain with obstacle (left) and history plot (right) of the objective function computed from the case of 16 384 elements below. Bottom: optimal configuration on polygonal grid consisting of 4096 (left) and 16 384 (right) elements.

Please cite this article in press as: P.F. Antonietti, et al., On the virtual element method for topology optimization on polygonal meshes: A numerical study, Computers and Mathematics with Applications (2017), http://dx.doi.org/10.1016/j.camwa.2017.05.025.

References

[1] L. Beirão da Veiga, A. Ern, Preface [Special issue—Polyhedral discretization for PDE], ESAIM Math. Model. Numer. Anal. 50 (3) (2016) 633–634.
[2] N. Bellomo, F. Brezzi, G. Manzini, Recent techniques for pde discretizations on polyhedral meshes, Math. Models Methods Appl. Sci. 24 (2014) 1453–1455. (special issue).
[3] L. Beirão da Veiga, F. Brezzi, A. Cangiani, G. Manzini, L.D. Marini, A. Russo, Basic principles of virtual element methods, Math. Models Methods Appl. Sci. 23 (1) (2013) 199–214.
[4] L. Beirão da Veiga, K. Lipnikov, G. Manzini, The Mimetic Finite Difference Method for Elliptic Problems, in: MS&A. Modeling, Simulation and Applications, vol. 11, Springer, Cham, 2014.
[5] K. Lipnikov, G. Manzini, M. Shashkov, Mimetic finite difference method, J. Comput. Phys. 257 (part B) (2014) 1163–1227.
[6] L. Beirão da Veiga, F. Brezzi, L.D. Marini, A. Russo, Virtual element method for general second-order elliptic problems on polygonal meshes, Math. Models Methods Appl. Sci. 26 (4) (2016) 729–750.
[7] M.F. Benedetto, S. Berrone, A. Borio, S. Pieraccini, S. Scialò, Order preserving SUPG stabilization for the virtual element formulation of advection-diffusion problems, Comput. Methods Appl. Mech. Engrg. 311 (2016) 18–40.
[8] L. Beirão da Veiga, F. Brezzi, L.D. Marini, Virtual elements for linear elasticity problems, SIAM J. Numer. Anal. 51 (2) (2013) 794–812.
[9] A.L. Gain, C. Talischi, G.H. Paulino, On the virtual element method for three-dimensional linear elasticity problems on arbitrary polyhedral meshes, Comput. Methods Appl. Mech. Engrg. 282 (2014) 132–160.
[10] L. Beirão da Veiga, C. Lovadina, D. Mora, A virtual element method for elastic and inelastic problems on polytope meshes, Comput. Methods Appl. Mech. Engrg. 295 (2015) 327–346.
[11] F. Brezzi, L.D. Marini, Virtual element methods for plate bending problems, Comput. Methods Appl. Mech. Engrg. 253 (2013) 455–462.
[12] C. Chinosi, L.D. Marini, Virtual Element Method for fourth order problems: L^2-estimates, Comput. Math. Appl. 72 (8) (2016) 1959–1967.
[13] P.F. Antonietti, L. Beirão da Veiga, S. Scacchi, M. Verani, A C^1 virtual element method for the Cahn-Hilliard equation with polygonal meshes, SIAM J. Numer. Anal. 54 (1) (2016) 34–56.
[14] P.F. Antonietti, L. Beirão da Veiga, D. Mora, M. Verani, A stream virtual element formulation of the Stokes problem on polygonal meshes, SIAM J. Numer. Anal. 52 (1) (2014) 386–404.
[15] L. Beirão da Veiga, C. Lovadina, G. Vacca, Divergence free Virtual Elements for the Stokes problem on polygonal meshes, October 2015. ArXiv e-prints: arxiv:1510.01655.
[16] I. Perugia, P. Pietra, A. Russo, A plane wave virtual element method for the Helmholtz problem, ESAIM Math. Model. Numer. Anal. 50 (3) (2016) 783–808.
[17] G. Vacca, L. Beirão da Veiga, Virtual element methods for parabolic problems on polygonal meshes, Numer. Methods Partial Differential Equations 31 (6) (2015) 2110–2134.
[18] D. Mora, G. Rivera, R. Rodríguez, A virtual element method for the Steklov eigenvalue problem, Math. Models Methods Appl. Sci. 25 (8) (2015) 1421–1445.
[19] F. Gardini, G. Vacca, Virtual Element Method for Second Order Elliptic Eigenvalue Problems, October 2016. ArXiv e-prints: arxiv:1610.03675.
[20] M.F. Benedetto, S. Berrone, S. Pieraccini, S. Scialò, The virtual element method for discrete fracture network simulations, Comput. Methods Appl. Mech. Engrg. 280 (2014) 135–156.
[21] F. Brezzi, R.S. Falk, L. Donatella Marini, Basic principles of mixed virtual element methods, ESAIM Math. Model. Numer. Anal. 48 (4) (2014) 1227–1240.
[22] L. Beirão da Veiga, F. Brezzi, L.D. Marini, A. Russo, Mixed virtual element methods for general second order elliptic problems on polygonal meshes, ESAIM Math. Model. Numer. Anal. 50 (3) (2016) 727–747.
[23] F. Brezzi, L.D. Marini, Virtual element and discontinuous Galerkin methods, in: Recent Developments in Discontinuous Galerkin Finite Element Methods for Partial Differential Equations, in: IMA Vol. Math. Appl, vol. 157, Springer, Cham, 2014, pp. 209–221.
[24] L. Beirão da Veiga, F. Brezzi, L.D. Marini, A. Russo, $H(\mathrm{div})$ and $H(\mathbf{curl})$-conforming virtual element methods, Numer. Math. 133 (2) (2016) 303–332.
[25] L. Beirão da Veiga, A. Chernov, L. Mascotto, A. Russo, Basic principles of *hp* virtual elements on quasiuniform meshes, Math. Models Methods Appl. Sci. 26 (8) (2016) 1567–1598.
[26] L. Beirão da Veiga, F. Brezzi, L.D. Marini, A. Russo, Serendipity nodal vem spaces, Comput. & Fluids (2016).
[27] B. Ayuso de Dios, K. Lipnikov, G. Manzini, The nonconforming virtual element method, ESAIM Math. Model. Numer. Anal. 50 (3) (2016) 879–904.
[28] A. Cangiani, G. Manzini, O.J. Sutton, Conforming and nonconforming virtual element methods for elliptic problems, July 2015. ArXiv e-prints: arxiv:1507.03543.
[29] A. Cangiani, V. Gyrya, G. Manzini, The non-conforming virtual element method for the Stokes equations, August 2016. ArXiv e-prints: arxiv:1608.01210.
[30] J. Zhao, S. Chen, B. Zhang, The nonconforming virtual element method for plate bending problems, Math. Models Methods Appl. Sci. 26 (9) (2016) 1671–1687.
[31] P.F. Antonietti, G. Manzini, M. Verani, The fully nonconforming Virtual Element Method for Biharmonic problems, 2016. ArXiv e-prints: arxiv:1611.08736.
[32] C. Talischi, G.H. Paulino, A. Pereira, I.F.M. Menezes, Polygonal finite elements for topology optimization: A unifying paradigm, Internat. J. Numer. Methods Engrg. 82 (2010) 671–698.
[33] C. Talischi, G.H. Paulino, A. Pereira, I.F.M. Menezes, PolyTop: a Matlab implementation of a general topology optimization framework using unstructured polygonal finite element meshes, Struct. Multidiscip. Optim. 45 (3) (2012) 329–357.
[34] C. Talischi, G.H. Paulino, A. Pereira, I.F.M. Menezes, PolyMesher: a general-purpose mesh generator for polygonal elements written in Matlab, Struct. Multidiscip. Optim. 45 (3) (2012) 309–328.
[35] C. Talischi, A. Pereira, G.H. Paulino, I.F.M. Menezes, M.S. Carvalho, Polygonal finite elements for incompressible fluid flow, Internat. J. Numer. Methods Fluids 74 (2) (2014) 134–151.
[36] A.L. Gain, G.H. Paulino, L.S. Duarte, I.F.M. Menezes, Topology optimization using polytopes, Comput. Methods Appl. Mech. Engrg. 293 (2015) 411–430.
[37] T. Borrvall, J. Petersson, Topology optimization of fluids in Stokes flow, Internat. J. Numer. Methods Fluids 41 (1) (2003) 77–107.
[38] L. Beirão da Veiga, K. Lipnikov, A mimetic discretization of the Stokes problem with selected edge bubbles, SIAM J. Sci. Comput. 32 (2) (2010) 875–893.
[39] B. Ahmad, A. Alsaedi, F. Brezzi, L.D. Marini, A. Russo, Equivalent projectors for virtual element methods, Comput. Math. Appl. 66 (3) (2013) 376–391.
[40] K. Svanberg, Method of moving asymptotes - a new method for structural optimization, Internat. J. Numer. Methods Engrg. 24 (1897) 193–202.
[41] M.P. Bendsøe, O. Sigmund, Topology Optimization Theory, Methods and Applications, Springer, New York, 2003.
[42] O. Sigmund, J. Petersson, Numerical instabilities in topology optimization: a survey on procedures dealing with checkerboards, mesh-dependencies and local minima, Struct. Optim. 16 (1998) 68–75.
[43] C. Le, J. Norato, T.E. Bruns, C. Ha, D.D. Tortorelli, Stress-based topology optimization for continua, Struct. Multidiscip. Optim. 41 (2010) 605–620.
[44] M. Bruggi, P. Duysinx, A stress-based approach to the optimal design of structures with unilateral behavior of material or supports, Struct. Multidiscip. Optim. 48 (2013) 311–326.
[45] S.H. Jeong, S.H. Park, D.H. Choi, G.H. Yoon, Topology optimization considering static failure theories for ductile and brittle materials, Comput. Struct. 110–111 (2012) 116–132.

Please cite this article in press as: P.F. Antonietti, et al., On the virtual element method for topology optimization on polygonal meshes: A numerical study, Computers and Mathematics with Applications (2017), http://dx.doi.org/10.1016/j.camwa.2017.05.025.

[46] S.H. Jeong, S.H. Park, D.H. Choi, G.H. Yoon, Toward a stress-based topology optimization procedure with indirect calculation of internal finite element information, Comput. Math. Appl. 66 (6) (2013) 1065–1108.
[47] S.H. Jeong, S.H. Park, D.H. Choi, G.H. Yoon, Fatigue and static failure considerations using a topology optimization method, Appl. Math. Model. 39 (3–4) (2015) 1137–1162.
[48] B. Bourdin, Filters in topology optimization, Internat. J. Numer. Methods Engrg. 50 (2001) 2143–2158.
[49] O. Sigmund, P.M. Clausen, Topology optimization using a mixed formulation: an alternative way to solve pressure load problems, Comput. Methods Appl. Mech. Engrg. 196 (2017) 1874–1889.
[50] M. Bruggi, P. Venini, Topology optimization of incompressible media using mixed finite elements, Comput. Methods Appl. Mech. Engrg. 196 (33–34) (2007) 3151–3164.
[51] M. Bruggi, Topology optimization with mixed finite elements on regular grids, Comput. Methods Appl. Mech. Engrg. 305 (2016) 133–153.
[52] M. Bruggi, M. Verani, A fully adaptive topology optimization algorithm with goal–oriented error control, Comput. Struct. 89 (2011) 1481–1493.
[53] P. Morin, R.H. Nochetto, M.S. Pauletti, M. Verani, Adaptive finite element method for shape optimization, ESAIM Control Optim. Calc. Var. 18 (4) (2012) 1122–1149.
[54] G.H. Yoon, Topology optimization for stationary fluid–structure interaction problems using a new monolithic formulation, Internat. J. Numer. Methods Engrg. 82 (5) (2010) 591–616.

Please cite this article in press as: P.F. Antonietti, et al., On the virtual element method for topology optimization on polygonal meshes: A numerical study, Computers and Mathematics with Applications (2017), http://dx.doi.org/10.1016/j.camwa.2017.05.025.